Cross Euclidean-to-Riemannian Metric Learning with Application to Face Recognition from Video

Zhiwu Huang ⓘ, *Member, IEEE*, Ruiping Wang ⓘ, *Member, IEEE*, Shiguang Shan ⓘ, *Senior Member, IEEE*, Luc Van Gool, *Member, IEEE*, and Xilin Chen, *Fellow, IEEE*

Abstract—Riemannian manifolds have been widely employed for video representations in visual classification tasks including video-based face recognition. The success mainly derives from learning a discriminant Riemannian metric which encodes the non-linear geometry of the underlying Riemannian manifolds. In this paper, we propose a novel metric learning framework to learn a distance metric across a Euclidean space and a Riemannian manifold to fuse average appearance and pattern variation of faces within one video. The proposed metric learning framework can handle three typical tasks of video-based face recognition: Video-to-Still, Still-to-Video and Video-to-Video settings. To accomplish this new framework, by exploiting typical Riemannian geometries for kernel embedding, we map the source Euclidean space and Riemannian manifold into a common Euclidean subspace, each through a corresponding high-dimensional Reproducing Kernel Hilbert Space (RKHS). With this mapping, the problem of learning a cross-view metric between the two source heterogeneous spaces can be converted to learning a single-view Euclidean distance metric in the target common Euclidean space. By learning information on heterogeneous data with the shared label, the discriminant metric in the common space improves face recognition from videos. Extensive experiments on four challenging video face databases demonstrate that the proposed framework has a clear advantage over the state-of-the-art methods in the three classical video-based face recognition scenarios.

Index Terms—Riemannian manifold, video-based face recognition, cross Euclidean-to-Riemannian metric learning

◆

1 INTRODUCTION

Dᴜᴇ to robustness against varying imaging conditions, Riemannian manifolds have proven powerful representations for video sequences in many branches of computer vision. Two of the most popular Riemannian structures are the manifold of linear subspaces (i.e., Grassmann manifold) and the manifold of Symmetric Positive Definite (SPD) matrices. From a different perspective, these Riemannian representations can be related to modeling a video with a multivariate Gaussian distribution, characterized by its mean and covariance matrix. In the case of the Grassmann manifold, the distances between subspaces can be reduced to distances between multivariate Gaussian distributions by treating linear subspaces as the flattened limit of a zero-mean, homogeneous factor analyzer distribution [1]. In the case of the SPD manifold, a sequence of video

frames is represented as the covariance matrix of the image features of frames [2], [3], which therefore essentially encodes a zero-mean Gaussian distribution of the image features. In [4], [5], each video is modeled as a Gaussian distribution with non-zero mean and covariance matrix, which can be combined to construct an SPD matrix, and thus also resides on a specific SPD manifold [6], [7].

The success of Riemannian representations in visual recognition is mainly due to the learning of more discriminant metrics, which encode Riemannian geometry of the underlying manifolds. For example, by exploiting the geometry of the Grassmann manifolds, [8] proposed Grassmann kernel functions to extend the existing Kernel Linear Discriminant Analysis [9] to learn a metric for Grassmannian representations. In [10], a new method is presented to learn a Riemannian metric on a Grassmann manifold by performing Riemannian geometry-aware dimensionality reduction from the original Grassmann manifold to a lower-dimensional, more discriminative Grassmann manifold where more favorable classification can be achieved. To learn a discriminant metric for SPD representations, [2] derived a kernel function that explicitly maps the SPD representations from the SPD manifold to a Euclidean space where a traditional metric learning method such as Partial Least Squares [11] can be applied. In [12], an approach is proposed to search for a projection that yields a low-dimensional SPD manifold with maximum discriminative power, encoded via an affinity-weighted similarity measure based on Riemannian metrics on the SPD manifold.

- *Z. Huang and L. Van Gool are with Computer Vision Lab (CVL), Swiss Federal Institute of Technology (ETH), Zurich 8092, Switzerland. L. Van Gool is also with the VISICS lab of the Katholieke Universiteit (KU), Leuven 3000, Belgium. E-mail: {zhiwu.huang, vangool}@vision.ee.ethz.ch.*
- *R. Wang, S. Shan, and X. Chen are with the Key Lab of Intelligent Information Processing of Chinese Academy of Sciences (CAS), Institute of Computing Technology (ICT), Beijing 100190, China. S. Shan is also with the CAS Center for Excellence in Brain Science and Intelligence Technology. E-mail: {wangruiping, sgshan, xlchen}@ict.ac.cn.*

In this paper, we focus on studying the application of Riemannian metric learning to the problem of video-based face recognition, which identifies a subject with his/her face video sequences. Generally speaking, there exist three typical tasks of video-based face recognition, i.e., Video-to-Still (V2S), Still-to-Video (S2V) and Video-to-Video (V2V) face identification/verification. Specifically, the task of V2S face recognition matches a query video sequence against still face images, which are typically taken in a controlled setting. This task commonly occurs in watch list screening systems. In contrast, in the task of S2V face recognition, a still face image is queried against a database of video sequences, which can be applied to locate a person of interest by searching his/her identity in the stored surveillance videos. The third task, i.e., V2V face recognition, looks for the same face in input video sequences among a set of target video sequences. For example, one could track a person by matching his/her video sequences recorded somewhere against the surveillance videos taken elsewhere.

To handle the tasks of video-based face recognition, state-of-the-art deep feature learning methods [13], [14], [15], [16], [17] typically adopt mean pooling strategy to fuse deep features from single frames within one face video. However, in addition to the first-order mean pooling, as studied in many works such as [1], [4], [5], [18], [19], the pattern variation (i.e., second-order pooling) of videos provides yet an important complementary cue for video-based face recognition. With this motivation in mind, we propose a new metric learning scheme across a Euclidean space and a Riemannian manifold to match/fuse appearance mean and patter variation (i.e., first- and second-order poolings) for still images and video sequences. In particular, the learning scheme employs either raw or even deeply learned feature vectors (i.e., Euclidean data) from still facial images, while representing the faces within one video sequence with both their appearance mean (i.e., Euclidean data) and pattern variation models that are typically treated as Riemannian data. Benefited from the new architecture, the three typical video-based face recognition tasks can be uniformly tackled. Compared with the previous version [20] that can only handle V2S/S2V face recognition with pattern variation modeling on videos, this paper mainly makes two technical improvements:

- To improve the V2S/S2V face recognition task, the new framework represents each video simultaneously with appearance mean and pattern variation models, and derives a more generalized cross Euclidean and Riemannian metric learning scheme to match still images and video sequences.
- The original framework is also extended to handle the task of V2V face recognition. To this end, the objective function of the framework is adapted to fuse Euclidean data (i.e., appearance mean) and Riemannian data (i.e., pattern variation) of videos in a unified framework.

The key challenge of learning Euclidean-to-Riemannian metric learning is the essentially heterogeneous properties of the processed underlying data spaces, i.e., Euclidean spaces and Riemannian manifolds, which respect totally different geometrical structures and thus are equipped with
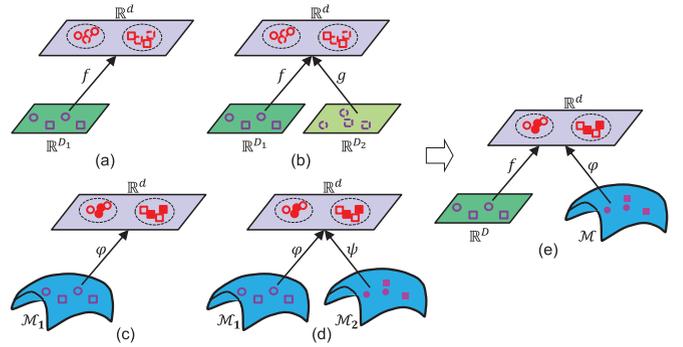

Fig. 1. Conceptual illustration of traditional Euclidean metric learning (a), Euclidean-to-Euclidean metric learning (b), Riemannian metric learning (c), Riemannian-to-Riemannian metric learning (d) and the proposed cross Euclidean-to-Riemannian metric learning (e). $\mathbb{R}^{D_1}/\mathbb{R}^{D_2}$, $\mathcal{M}/\mathcal{M}_1/\mathcal{M}_2$ and $\mathbb{R}^d$ indicate a Euclidean space, a Riemannian manifold and a common subspace, respectively. f/g, φ/ψ denote linear and non-linear transformations, and different shapes (i.e., circles and rectangles) represent classes.

different metrics, i.e., Euclidean distance and Riemannian metric respectively. As a result, applying most of traditional metric learning methods in Figs. 1a, 1b, 1c and 1d will totally break down in the context of learning a metric across a Euclidean space and a Riemannian manifold. For example, Euclidean-to-Euclidean metric learning Fig. 1b merely learns a discriminative distance metric between two Euclidean spaces with different data domain settings, while Riemannian-to-Riemannian metric learning Fig. 1d only explores a discriminative function across two homogeneous Riemannian manifolds. Hence, in the metric learning theory, this work mainly brings the following three innovations:

- As depicted in Fig. 1e, a novel heterogeneous metric learning framework is developed to match/fuse Euclidean and Riemannian representations by designing a new objective function well performing across Euclidean-Riemannian spaces. To the best of our knowledge, it is one of the first attempts to learn the metric across Euclidean and Riemannian spaces.
- The proposed metric learning scheme can accommodate a group of typical non-Euclidean (Riemannian) representations widely used in vision problems, e.g., linear subspaces, affine subspaces and SPD matrices. Thus, it is a general metric learning framework to study the problem of fusing/matching hybrid Euclidean and Riemannian data.

2 RELATED WORK

In this section we review relevant Euclidean metric learning and Riemannian metric learning methods. In addition, we also introduce existing applications of Riemannian metric learning to the problem of video-based face recognition.

2.1 Euclidean Metric Learning

In conventional techniques to learn a metric in a Euclidean space, the learned distance metric is usually defined as a Mahalanobis distance, which is the squared Euclidean distance after applying the learned linear transformation(s) to the original Euclidean space(s). According to the number of the source Euclidean spaces, traditional metric learning

methods can be categorized into Euclidean metric learning and Euclidean-to-Euclidean metric learning.

As shown in Fig. 1a, the Euclidean metric learning methods [21], [22], [23], [24], [25] intend to learn a metric or a transformation f of object features from a source Euclidean space $\mathbb{R}^D$ to a target Euclidean space $\mathbb{R}^d$. For example, [22] introduced an information-theoretic formulation to learn a metric in one source Euclidean space. In [24], a metric learning method was proposed to learn a transformation from one Euclidean space to a new one for the K-nearest neighbor algorithm by pulling neighboring objects of the same class closer together and pushing others further apart. In [25], an approach was presented to learn a distance metric between (realistic and virtual) data in a single Euclidean space for the definition of a more appropriate point-to-set distance in the application of point-to-set classification.

In contrast, as depicted in Fig. 1b, the Euclidean-to-Euclidean metric learning methods [26], [27], [28], [29], [30], [31], [32] are designed to learn a cross-view metric or multiple transformations f, g mapping object features from multiple source Euclidean spaces, say $\mathbb{R}^{D_1}$, $\mathbb{R}^{D_2}$, to a target common subspace $\mathbb{R}^d$. For instance, [29] proposed a metric learning method to seek multiple projections under a neighborhood preserving constraint for multi-view data in multiple Euclidean spaces. In [30], a multiple kernel/metric learning technique was applied to integrate different object features from multiple Euclidean spaces into a unified Euclidean space. In [32], a metric learning method was developed to learn two projections from two different Euclidean spaces to a common subspace by integrating the structure of cross-view data into a joint graph regularization.

2.2 Riemannian Metric Learning

Riemannian metric learning pursues discriminant functions on Riemannian manifold(s) in order to classify the Riemannian representations more effectively. In general, existing Riemannian metric learning Fig. 1c and Riemannian-to-Riemannian metric learning Fig. 1d adopt one of the following three typical schemes to achieve a more desirable Riemannian metric on/across Riemannian manifold(s).

The first Riemannian metric learning scheme [33], [34], [35], [36], [37], [38] typically first flattens the underlying Riemannian manifold via tangent space approximation, and then learns a discriminant metric in the resulting tangent (Euclidean) space by employing traditional metric learning methods. However, the map between the manifold and the tangent space is locally diffeomorphic, which inevitably distorts the original Riemannian geometry. To address this problem, LogitBoost on SPD manifolds [33] was introduced, by pooling the resulting classifiers in multiple approximated tangent spaces on the calculated Karcher mean on Riemannian manifolds. Similarly, a weighted Riemannian locality preserving projection is exploited by [37] during boosting for classification on Riemannian manifolds.

Another family of Riemannian metric learning methods [1], [2], [3], [4], [8], [39], [40], [41], [42] derives Riemannian metric based kernel functions to embed the Riemannian manifolds into a high-dimensional Reproducing Kernel Hilbert space (RKHS). As an RKHS respects Euclidean geometry, this learning scheme enables the traditional kernel-based metric learning methods to work in the resulting

RKHS. For example, in [1], [3], [8], [39], the projection metric based kernel and its extensions were introduced to map the underlying Grassmann manifold to an RKHS, where kernel learning algorithms developed in vector spaces can be extended to their counterparts. To learn discriminant data on the SPD manifolds, [2], [3], [4], [40], [41], [42] exploited some well-studied Riemannian metrics such as the Log-Euclidean metric [43], to derive positive definite kernels on manifolds that permit to embed a given manifold with a corresponding metric into a high-dimensional RKHS.

The last kind of Riemannian metric learning [10], [12], [44], [45] learns the metric by mapping the original Riemannian manifold to another one equipped with the same Riemannian geometry. For instance, in [12], a metric learning algorithm was introduced to map a high-dimensional SPD manifold into a lower-dimensional, more discriminant one. This work proposed a graph embedding formalism with an affinity matrix that encodes intra-class and inter-class distances based on affine-invariant Riemannian metrics [46], [47] on the SPD manifold. Analogously, on the Grassmann manifold, [10] proposed a new Riemannian metric learning to learn a Mahalanobis-like matrix that can be decomposed into a manifold-to-manifold transformation for geometry-aware dimensionality reduction.

In contrast to Riemannian metric learning performed on a single Riemannian manifold, Riemannian-to-Riemannian metric learning [19], [48] typically learns multiple Riemannian metrics across different types of Riemannian manifolds by employing the second Riemannian metric learning scheme mentioned above. For example, in [48], multiple Riemannian manifolds were first mapped into multiple RKHSs, and a feature combining and selection method based on a traditional Multiple Kernel Learning technique was then introduced to optimally combine the multiple transformed data lying in the resulting RKHSs. Similarly, [19] adopted multiple traditional metric learning methods to fuse the classification scores on multiple Riemannian representations by employing Riemannian metric based kernels on their underlying Riemannian manifolds.

2.3 Riemannian Metric Learning Applied to Video-Based Face Recognition

State-of-the-art methods [1], [2], [4], [5], [8], [12], [18], [35], [45], [49] typically model each video sequence of faces with a variation model (e.g., linear subspace, affine subspace and SPD matrices) and learn a discriminant Riemannian metric on the underlying Riemannian manifold for robust video-based face recognition. For example, [8] represented each set of video frames by a linear subspace of their image features. By exploiting the geometry of the underlying Grassmann manifold of linear subspaces, they extended the Kernel Linear Discriminant Analysis method to learn discriminative linear subspaces. As studied in [1], image sets are more robustly modeled by affine subspaces, each of which is obtained by adding an offset (i.e, the data mean) to one linear subspace. Analogously to [8], an affine Grassmann manifold and its Riemannian geometry were exploited by [1] for affine subspace discriminant learning. In [2], each video is modeled as a covariance matrix, which is then treated as an SPD matrix residing on the SPD manifold. To learn discriminative SPD matrices, they applied
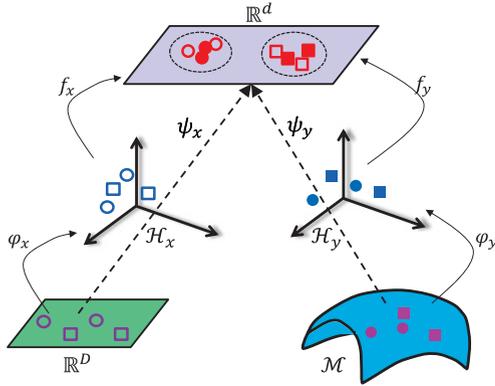
Fig. 2. Overview of the proposed Cross Euclidean-to-Riemannian Metric Learning (CERML) framework. $\mathbb{R}^D$, $\mathcal{M}$, $\mathcal{H}_x/\mathcal{H}_y$, $\mathbb{R}^d$ represent a Euclidean space, a Riemannian manifold, a Hilbert space and a common subspace respectively. f_x/f_y, ψ_x/ψ_y denote linear and nonlinear transformation functions, and different shapes represent classes.

traditional discriminant analysis methods such as Partial Least Squares on the manifold of SPD matrices. Accordingly, the success of these methods mainly derives from the effective video modeling with Riemannian representations and discriminant metric learning on such Riemannian data.

3　CROSS EUCLIDEAN-TO-RIEMANNIAN METRIC LEARNING

In this section, we first formulate the new problem of Cross Euclidean-to-Riemannian Metric Learning (CERML), and then present its objective function. In the end, we develop an optimization algorithm to solve the objective function.

3.1　Problem Formulation

Let $X = \{\boldsymbol{x}_1, \boldsymbol{x}_2, \ldots, \boldsymbol{x}_m\}, \boldsymbol{x}_i \in \mathbb{R}^D$ be a set of Euclidean data with class labels $\{l_1^x, l_2^x, \ldots, l_m^x\}$ and $Y = \{\boldsymbol{y}_1, \boldsymbol{y}_2, \ldots, \boldsymbol{y}_n\}, \boldsymbol{y}_j \in \mathcal{M}$ be a set of Riemannian representations with class labels $\{l_1^y, l_2^y, \ldots, l_n^y\}$, where $\boldsymbol{y}_j$ come as a certain type of Riemannian representations such as linear subspaces, affine subspaces, or SPD matrices.

Given one pair of a Euclidean point $\boldsymbol{x}_i$ and a Riemannian point $\boldsymbol{y}_j$, we use $d(\boldsymbol{x}_i, \boldsymbol{y}_j)$ to represent their distance. To achieve an appropriate distance metric between them for better discrimination, we propose to learn two transformation functions ψ_x and ψ_y, which respectively map the Euclidean points and Riemannian points to a common Euclidean subspace. In the common subspace, the learned distance metric between the involved pair of heterogeneous data can be reduced to the classical Euclidean distance as

$$d(\boldsymbol{x}_i, \boldsymbol{y}_j) = \sqrt{(\psi_x(\boldsymbol{x}_i) - \psi_y(\boldsymbol{y}_j))^T (\psi_x(\boldsymbol{x}_i) - \psi_y(\boldsymbol{y}_j))}. \quad (1)$$

However, as the source Euclidean space $\mathbb{R}^D$ and Riemannian manifold $\mathcal{M}$ differ too much in terms of geometrical data structure, it is difficult to employ linear transformations to map them into the common target Euclidean subspace $\mathbb{R}^d$. This motivates us to first transform the Riemannian manifold to a flat Euclidean space so that the heterogeneity between this flattened space and the source Euclidean space reduces. To this end, there exist two strategies: one is tangent space embedding, and the other is Reproducing Kernel Hilbert

Space (RKHS) embedding. The first strategy pursues an appropriate tangent space to approximate the local geometry of the Riemannian manifold. In contrast, the second strategy exploits typical Riemannian metrics based kernel functions to encode Riemannian geometry of the underlying manifold. As evidenced by the theory of kernel methods in Euclidean spaces, compared with the tangent space embedding scheme, the RKHS embedding yields much richer high-dimensional representations of the original data, making visual classification tasks easier.

With this idea in mind, and as shown in Fig. 2, the proposed framework of Cross Euclidean-to-Riemannian Metric Learning first derives the kernel functions based on typical Euclidean and Riemannian metrics to define the inner product of the implicit non-linear transformations φ_x and φ_y, which respectively map the Euclidean space $\mathbb{R}^D$ and the Riemannian manifold $\mathcal{M}$ into two RKHSs $\mathcal{H}_x$, $\mathcal{H}_y$. After the kernel space embedding, two mappings f_x, f_y are learned from the two RKHSs to the target common subspace. Thus, the final goal of this new framework is to employ the two mappings ψ_x and ψ_y to transform the original Euclidean data and Riemannian data into the common subspace $\mathbb{R}^d$, where the distance metric between each pair of Euclidean data point and Riemannian data point is reduced to the classical Euclidean distance defined in Eq. (1). In particular, the two linear projections can be represented as $f_x(\boldsymbol{x}_i) = V_x^T \boldsymbol{x}_i$, $f_y(\boldsymbol{y}_j) = V_y^T \boldsymbol{y}_j$, where V_x^T, V_y^T are two linear projection matrices. Inspired by the classical kernel techniques, we employ the corresponding kernel functions to derive the inner products of these two non-linear transformations as $\langle \varphi_x(\boldsymbol{x}_i), \varphi_x(\boldsymbol{x}_j) \rangle = K_x(\boldsymbol{x}_i, \boldsymbol{x}_j)$, $\langle \varphi_y(\boldsymbol{y}_i), \varphi_y(\boldsymbol{y}_j) \rangle = K_y(\boldsymbol{y}_i, \boldsymbol{y}_j)$, where K_x, K_y are the kernel matrices involved. By parameterizing the inner products in the two RKHSs, the formulations of the two final mapping functions ψ_x and ψ_y can be achieved by $\psi_x(\boldsymbol{x}_i) = W_x^T K_{x_{.i}}$, $\psi_y(\boldsymbol{y}_j) = W_y^T K_{y_{.j}}$, where $K_{x_{.i}}, K_{y_{.i}}$ are respectively the ith columns of the kernel matrices K_x, K_y. Accordingly, the distance metric Eq. (1) between a pair of a Euclidean point $\boldsymbol{x}$ and a Riemannian representation $\boldsymbol{y}$ can be further formulated as

$$d(\boldsymbol{x}_i, \boldsymbol{y}_j) = \sqrt{(W_x^T K_{x_{.i}} - W_y^T K_{y_{.j}})^T (W_x^T K_{x_{.i}} - W_y^T K_{y_{.j}})}. \quad (2)$$

Additionally, according to the above mapping mode, the distance metric between each pair of transformed homogeneous data points in the common Euclidean subspace can also be achieved as

$$d_x(\boldsymbol{x}_i, \boldsymbol{x}_j) = \sqrt{(W_x^T K_{x_{.i}} - W_x^T K_{x_{.j}})^T (W_x^T K_{x_{.i}} - W_x^T K_{x_{.j}})}, \quad (3)$$

$$d_y(\boldsymbol{y}_i, \boldsymbol{y}_j) = \sqrt{(W_y^T K_{y_{.i}} - W_y^T K_{y_{.j}})^T (W_y^T K_{y_{.i}} - W_y^T K_{y_{.j}})}, \quad (4)$$

where the specific forms of K_x and K_y will be presented in the following.

Now, we need to define the kernel functions $K_x(\boldsymbol{x}_i, \boldsymbol{x}_j)$, $K_y(\boldsymbol{y}_i, \boldsymbol{y}_j)$ for Euclidean data and Riemannian representations. For the Euclidean data, without loss of generality, we exploit the Radial Basis Function (RBF) kernel, which is one of the most popular positive definite kernels. Formally,

given a pair of data point x_i, x_j in Euclidean space, the kernel function is defined as

$$K_x(x_i, x_j) = exp(-\|x_i - x_j\|^2/2\sigma_x^2), \qquad (5)$$

which actually employs the Euclidean distance between two Euclidean points x_i and x_j.

As for the Riemannian representations, since they are commonly defined on a specific type of Riemannian manifold that respects a non-Euclidean geometry [1], [2], [8], the above kernel function formulation will fail. So, it has to be generalized to Riemannian manifolds. For this purpose, given two elements y_i, y_j on a Riemannian manifold, we formally define a generalized kernel function for them as

$$K_y(y_i, y_j) = exp(-d^2(y_i, y_j)/2\sigma_y^2). \qquad (6)$$

The kernel function performed on Riemannian representations actually takes the form of a Gaussian function (note that we also study the linear kernel case in the supplementary material, which can be found on the Computer Society Digital Library at http://doi.ieeecomputersociety.org/10.1109/TPAMI.2017.2776154). The most important component in such a kernel function is $d(y_i, y_j)$, which defines the distance between one pair of Riemannian points on the underlying Riemannian manifold. Next, this distance is discussed for three typical Riemannian representations, i.e., Grassmannian data, affine Grassmannian data and SPD data.

3.1.1 For Grassmannian Representations

As studied in [1], [3], [8], [39], [50], each Riemannian representation on a Grassmann manifold $\mathcal{G}(d, D)$ refers to a d-dimensional linear subspace of $\mathbb{R}^D$. The linear subspace can be represented by its orthonormal basis matrix U that is formed by the d leading eigenvectors corresponding to the d largest eigenvalues of the covariance matrix of one Euclidean data set. On a Grassmann manifold, one of the most popular Riemannian metrics is the projection metric [50]. Formally, for one pair of data y_i, y_j on the Grassmannian, their distance is measured by the projection metric

$$d(y_i, y_j) = 2^{-1/2}\|U_iU_i^T - U_jU_j^T\|_{\mathcal{F}}, \qquad (7)$$

where $\|\cdot\|_{\mathcal{F}}$ denotes the matrix Frobenius norm.

3.1.2 For Affine Grassmannian Representations

In contrast to the Grassmannian representation, each affine Grassmannian point is an element on an affine Grassmann manifold, which is the space of d-dimensional affine subspaces named affine Grassmann manifold $\mathcal{AG}(d, D)$. Therefore, each Riemannian representation on $\mathcal{AG}(d, D)$ is an affine subspace spanned by an orthonormal matrix U adding the offset μ (i.e., the mean) from the origin. On the affine Grassmann manifold, [1] defined a similarity function as $tr(U_iU_i^TU_jU_j^T) + \mu_i^T(I - U_iU_i^T)(I - U_jU_j^T)\mu_j$ between pairs of data points. Alternatively, we extend the similarity function to a distance metric between two Riemannian data y_i, y_j on the affine manifold as

$$
\begin{aligned}
d(y_i, y_j) = 2^{-1/2}(&\|U_iU_i^T - U_jU_j^T\|_{\mathcal{F}} \\
&+ \|(I - U_iU_i^T)\mu_i - (I - U_jU_j^T)\mu_j\|_{\mathcal{F}}),
\end{aligned} \qquad (8)
$$

where $I \in \mathbb{R}^{D \times D}$ is the identity matrix.

3.1.3 For SPD Representations

Each SPD representation is an element of the manifold of Symmetric Positive Definite matrices C of size $D \times D$. As studied in [2], [42], [43], [46], the set of SPD matrices yields a Riemannian manifold $\mathbb{S}_+^D$ when endowing a specific Riemannian metric. One of the most commonly used SPD Riemannian metrics is the Log-Euclidean metric [43] due to its effectiveness in encoding the true Riemannian geometry by reducing the manifold to a flat tangent space at the identity matrix. Formally, on the Riemannian SPD manifold, the Log-Euclidean distance metric between two elements y_i, y_j is given by classical Euclidean computations in the domain of SPD matrix logarithms as

$$d(y_i, y_j) = \|\log(C_i) - \log(C_j)\|_{\mathcal{F}}, \qquad (9)$$

where $\log(C) = U\log(\Sigma)U^T$ with $C = U\Sigma U^T$ being the eigen-decomposition of the SPD matrix C.

Similar to our prior work [20], we denote the proposed CERML working in the three studied settings by CERML-EG, CERML-EA and CERML-ES, respectively. By studying the Riemannian metrics defined in Eqs. (7), (8) and (9), the kernel function corresponding to the specific type of Riemannian manifold can be derived by employing Eq. (6). However, according to Mercer's theorem, only positive definite kernels yield valid RKHS. To achieve this, by employing the approach developed in [42], we can easily prove the positive definiteness of these Gaussian kernels defined on the resulting Riemannian manifolds. As for the details to prove their positive definiteness, readers are referred to [42].

3.2 Objective Function

From Eqs. (2), (3), and (4), we find that the CERML contains two parameter transformation matrices W_x, W_y. In order to learn a discriminant metric between heterogeneous data, we formulate the objective function of this new framework to optimize the two matrices W_x, W_y in the following:

$$
\begin{aligned}
&\min_{W_x, W_y} J(W_x, W_y) \\
&= \min_{W_x, W_y} \{D(W_x, W_y) + \lambda_1 G(W_x, W_y) + \lambda_2 T(W_x, W_y)\},
\end{aligned}
$$

$$(10)$$

where $D(W_x, W_y)$ is the distance constraint defined on the collections of similarity and dissimilarity constraints. $G(W_x, W_y)$ and $T(W_x, W_y)$ are, respectively, a geometry constraint and a transformation constraint, both of which are regularizations defined on the target transformation matrices W_x, W_y. $\lambda_1 > 0, \lambda_2 > 0$ are balancing parameters.

Distance Constraint $D(W_x, W_y)$. This constraint is defined so that the distances between the Euclidean data and the Riemannian data—with the similarity (/dissimilarity) constraints—are minimized (/maximized). In this paper, we adopt a classical expression of the sum of squared distances to define this constraint as

$$D(\boldsymbol{W}_x, \boldsymbol{W}_y) = \frac{1}{2} \sum_{i=1}^{m} \sum_{j=1}^{n} \boldsymbol{A}(i,j) d^2(\boldsymbol{x}_i, \boldsymbol{y}_j),$$

$$\boldsymbol{A}(i,j) = \begin{cases} 1, & \text{if } l_i^x = l_j^y, \\ -1, & \text{if } l_i^x \neq l_j^y, \end{cases} \tag{11}$$

where $\boldsymbol{A}(i,j)$ indicates if the heterogeneous data $\boldsymbol{x}_i$ and $\boldsymbol{y}_j$ are relevant or irrelevant, as inferred from the class label. To balance the effect of similarity and dissimilarity constraints, we normalize the elements of A by averaging them over the total number of similar/dissimilar pairs respectively.

Geometry Constraint $G(\boldsymbol{W}_x, \boldsymbol{W}_y)$. This constraint aims to preserve Euclidean geometry and Riemannian geometry for the Euclidean and Riemannian points, respectively. Thus, it can be defined as: $G(\boldsymbol{W}_x, \boldsymbol{W}_y) = G_x(\boldsymbol{W}_x) + G_y(\boldsymbol{W}_y)$, which are Euclidean and Riemannian geometry preserving items formulated as

$$G_x(\boldsymbol{W}_x) = \frac{1}{2} \sum_{i=1}^{m} \sum_{j=1}^{m} \boldsymbol{A}_x(i,j) d_x^2(\boldsymbol{x}_i, \boldsymbol{x}_j),$$

$$\boldsymbol{A}_x(i,j) = \begin{cases} a_{ij}, & \text{if } l_i^x = l_j^x \text{ and } k_1(i,j), \\ -a_{ij}, & \text{if } l_i^x \neq l_j^x \text{ and } k_2(i,j), \\ 0, & \text{else}, \end{cases} \tag{12}$$

$$G_y(\boldsymbol{W}_y) = \frac{1}{2} \sum_{i=1}^{n} \sum_{j=1}^{n} \boldsymbol{A}_y(i,j) d_y^2(\boldsymbol{y}_i, \boldsymbol{y}_j),$$

$$\boldsymbol{A}_y(i,j) = \begin{cases} a_{ij}, & \text{if } l_i^y = l_j^y \text{ and } k_1(i,j), \\ -a_{ij}, & \text{if } l_i^y \neq l_j^y \text{ and } k_2(i,j), \\ 0, & \text{else}, \end{cases} \tag{13}$$

where $a_{ij} = exp(\|\hat{\boldsymbol{x}}_i - \hat{\boldsymbol{x}}_j\|^2/\sigma^2)$, $\hat{\boldsymbol{x}}$ indicates Euclidean data $\boldsymbol{x}$ or Riemannian data $\boldsymbol{y}$. $k_1(i,j)$ $(k_2(i,j))$ means data z_i is in the k_1 (k_2) neighborhood of data z_j or data z_j is in the k_1 (k_2) neighborhood of data z_i.

Transformation Constraint $T(\boldsymbol{W}_x, \boldsymbol{W}_y)$. Since Euclidean distance will be used in the target common subspace where all dimensions are treated uniformly, it is reasonable to require the feature vectors satisfy an isotropic distribution. Thus, this constraint can be expressed in terms of unit covariance

$$T(\boldsymbol{W}_x, \boldsymbol{W}_y) = \frac{1}{2} (\|\boldsymbol{W}_x^T \boldsymbol{K}_x\|_{\mathcal{F}}^2 + \|\boldsymbol{W}_y^T \boldsymbol{K}_y\|_{\mathcal{F}}^2), \tag{14}$$

where $\| \cdot \|_{\mathcal{F}}$ is the Frobenius norm.

3.3 Optimization Algorithm

To optimize the objective function Eq. (10), we develop an iterative optimization algorithm, which first applies the Fisher criterion of Fisher Discriminant Analysis (FDA) [51] to initialize the two transformation matrices $\boldsymbol{W}_x, \boldsymbol{W}_y$, and then employs a strategy of alternately updating their values.

Before introducing the optimization algorithm, we first rewrite Eqs. (11), (12) and (13) in matrix formulation as

$$D(\boldsymbol{W}_x, \boldsymbol{W}_y) = \frac{1}{2} (\boldsymbol{W}_x^T \boldsymbol{K}_x \boldsymbol{B}_x' \boldsymbol{K}_x^T \boldsymbol{W}_x + \boldsymbol{W}_y^T \boldsymbol{K}_y \boldsymbol{B}_y' \boldsymbol{K}_y^T \boldsymbol{W}_y \\ - 2\boldsymbol{W}_x^T \boldsymbol{K}_x \boldsymbol{A} \boldsymbol{K}_y^T \boldsymbol{W}_y), \tag{15}$$

$$G_x(\boldsymbol{W}_x) = \boldsymbol{W}_x^T \boldsymbol{K}_x \boldsymbol{B}_x \boldsymbol{K}_x^T \boldsymbol{W}_x - \boldsymbol{W}_x^T \boldsymbol{K}_x \boldsymbol{A}_x \boldsymbol{K}_x^T \boldsymbol{W}_x \\ = \boldsymbol{W}_x^T \boldsymbol{K}_x \boldsymbol{L}_x \boldsymbol{K}_x^T \boldsymbol{W}_x, \tag{16}$$

$$G_y(\boldsymbol{W}_y) = \boldsymbol{W}_y^T \boldsymbol{K}_y \boldsymbol{B}_y \boldsymbol{K}_y^T \boldsymbol{W}_y - \boldsymbol{W}_y^T \boldsymbol{K}_y \boldsymbol{A}_y \boldsymbol{K}_y^T \boldsymbol{W}_y \\ = \boldsymbol{W}_y^T \boldsymbol{K}_y \boldsymbol{L}_y \boldsymbol{K}_y^T \boldsymbol{W}_y, \tag{17}$$

where $\boldsymbol{B}_x'$, $\boldsymbol{B}_y'$, $\boldsymbol{B}_x$ and $\boldsymbol{B}_y$ are diagonal matrices with $\boldsymbol{B}_x'(i,i) = \sum_{j=1}^{n} \boldsymbol{A}(i,j)$, $\boldsymbol{B}_y'(j,j) = \sum_{i=1}^{m} \boldsymbol{A}(i,j)$, $\boldsymbol{B}_x(i,i) = \sum_{j=1}^{m} \boldsymbol{A}_x(i,j)$, $\boldsymbol{B}_y(i,i) = \sum_{j=1}^{n} \boldsymbol{A}_y(i,j)$.

Initialization. We define the within-class template $\boldsymbol{A}^w$ and between-class template $\boldsymbol{A}^b$ for $\boldsymbol{A}$ in Eq. (11) as

$$\boldsymbol{A}^w(i,j) = \begin{cases} 1, & \text{if } l_i^x = l_j^y, \\ 0, & \text{if } l_i^x \neq l_j^y, \end{cases} \quad \boldsymbol{A}^b(i,j) = \begin{cases} 0, & \text{if } l_i^x = l_j^y, \\ 1, & \text{if } l_i^x \neq l_j^y. \end{cases} \tag{18}$$

By substituting Eq. (18) into Eq. (15), the within-class template $D^w(\boldsymbol{W}_x, \boldsymbol{W}_y)$ and between-class template $D^b(\boldsymbol{W}_x, \boldsymbol{W}_y)$ for $D(\boldsymbol{W}_x, \boldsymbol{W}_y)$ in Eq. (11) can be computed as

$$D^w(\boldsymbol{W}_x, \boldsymbol{W}_y) = \frac{1}{2} (\boldsymbol{W}_x^T \boldsymbol{K}_x \boldsymbol{B}_x'^w \boldsymbol{K}_x^T \boldsymbol{W}_x + \boldsymbol{W}_y^T \boldsymbol{K}_y \boldsymbol{B}_y'^w \boldsymbol{K}_y^T \boldsymbol{W}_y \\ - 2\boldsymbol{W}_x^T \boldsymbol{K}_x \boldsymbol{Z}^w \boldsymbol{K}_y \boldsymbol{W}_y^T), \tag{19}$$

$$D^b(\boldsymbol{W}_x, \boldsymbol{W}_y) = \frac{1}{2} (\boldsymbol{W}_x^T \boldsymbol{K}_x \boldsymbol{B}_x'^b \boldsymbol{K}_x^T \boldsymbol{W}_x + \boldsymbol{W}_y^T \boldsymbol{K}_y \boldsymbol{B}_y'^b \boldsymbol{K}_y^T \boldsymbol{W}_y \\ - 2\boldsymbol{W}_x^T \boldsymbol{K}_x \boldsymbol{Z}^b \boldsymbol{K}_y \boldsymbol{W}_y^T). \tag{20}$$

Likewise, we achieve the within-class and between-class templates for G_x and G_y in Eqs. (12) and (13) respectively denoted by G_x^w, G_x^b, G_y^w, G_y^b. For the sake of clarity, more details are given in the supplementary material, available online.

Then we can initialize $\boldsymbol{W}_x$ and $\boldsymbol{W}_y$ by maximizing the sum of between-class templates while minimizing the sum of within-class templates with the Fisher criterion of the traditional Fisher Discriminant Analysis [51]

$$\max_{\boldsymbol{W}_x, \boldsymbol{W}_y} \{D^b(\boldsymbol{W}_x, \boldsymbol{W}_y) + \lambda_1 G^b(\boldsymbol{W}_x, \boldsymbol{W}_y)\},$$
$$s.t. \quad D^w(\boldsymbol{W}_x, \boldsymbol{W}_y) + \lambda_1 G^w(\boldsymbol{W}_x, \boldsymbol{W}_y) = 1, \tag{21}$$

where $G^b(\boldsymbol{W}_x, \boldsymbol{W}_y) = G_x^b(\boldsymbol{W}_x, \boldsymbol{W}_y) + G_y^b(\boldsymbol{W}_x, \boldsymbol{W}_y)$, $G^w(\boldsymbol{W}_x, \boldsymbol{W}_y) = G_x^w(\boldsymbol{W}_x, \boldsymbol{W}_y) + G_y^w(\boldsymbol{W}_x, \boldsymbol{W}_y)$. By transforming Eq. (21) into matrix formulation, the function for initialization can be further simplified as

$$\max \boldsymbol{W}^T \boldsymbol{M}^b \boldsymbol{W}, \quad s.t. \; \boldsymbol{W}^T \boldsymbol{M}^w \boldsymbol{W} = 1,$$
$$\Rightarrow \boldsymbol{M}^b \boldsymbol{W} = \lambda \boldsymbol{M}^w \boldsymbol{W}, \tag{22}$$

where

$$\boldsymbol{M}^b = \begin{bmatrix} \boldsymbol{K}_x \boldsymbol{R}_x^b \boldsymbol{K}_x^T & -\boldsymbol{K}_x \boldsymbol{Z}^b \boldsymbol{K}_y^T \\ -\boldsymbol{K}_y (\boldsymbol{Z}^b)^T \boldsymbol{K}_x^T & \boldsymbol{y} \boldsymbol{R}_y^b \boldsymbol{K}_y^T \end{bmatrix},$$

$$\boldsymbol{M}^w = \begin{bmatrix} \boldsymbol{K}_x \boldsymbol{R}_x^w \boldsymbol{K}_x^T & -\boldsymbol{K}_x \boldsymbol{Z}^w \boldsymbol{K}_y^T \\ -\boldsymbol{K}_y (\boldsymbol{Z}^w)^T \boldsymbol{K}_x^T & \boldsymbol{y} \boldsymbol{R}_y^w \boldsymbol{K}_y^T \end{bmatrix},$$

$\boldsymbol{W}^T = [\boldsymbol{W}_x^T, \boldsymbol{W}_y^T]$. Obviously, Eq. (22) is a standard generalized eigenvalue problem that can be solved using any eigensolvers.

Alternately Updating. We substitute Eqs. (15), (16), and (17) into the objective function $J(\boldsymbol{W}_x, \boldsymbol{W}_y)$ in Eq. (10) to

derive its matrix form. By differentiating $J(W_x, W_y)$ w.r.t. W_x and setting it to zero, we have the following equation:

$$\frac{\partial Q(W_x, W_y)}{\partial W_x} = K_x B_x' K_x^T W_x - K_x Z K_y^T W_y \\ + 2\lambda_1 K_x L_x K_x^T W_x + 2\lambda_2 K_x K_x^T W_x = 0. \quad (23)$$

Then by fixing W_y, the solution of W_x can be achieved as

$$W_x = (K_x(B_x' + 2\lambda_1 L_x + 2\lambda_2 I)K_x^T)^{-1} K_x A K_y^T W_y. \quad (24)$$

Likewise, the solution of W_y when W_x is fixed, can be obtained as

$$W_y = (K_y(B_y' + 2\lambda_1 L_y + 2\lambda_2 I)K_y^T)^{-1} K_y A K_x^T W_x. \quad (25)$$

We alternate the above updates of W_x and W_y for several iterations to search an optimal solution. While it is hard to provide a theoretical proof of uniqueness or convergence of the proposed iterative optimization, we empirically found our objective function Eq. (10) can converge to a desirable solution after only a few tens of iterations. The convergence characteristics are studied in more detail in the experiments.

4 APPLICATION TO VIDEO-BASED FACE RECOGNITION

In this section we present the application of the proposed Cross Euclidean-to-Riemannian Metric Learning to the three typical tasks of video-based face recognition, i.e., V2S, S2V and V2V settings.

4.1 V2S/S2V Face Recognition

As done in several state-of-the-art techniques [2], [4], [5], [8], [12], [18], [35], we represent a set of facial frames within one video with their appearance mean and variation model aforementioned (e.g., linear subspace) simultaneously. Therefore, the task of V2S/S2V face recognition can be formulated as the problem of matching Euclidean representations (i.e., feature vectors) of face images with the Euclidean data (i.e., feature mean) and Riemannian representation (i.e., feature variation) of faces from videos. Formally, the Euclidean data of a face image is written as $X = \{x_1, x_2, \ldots, x_m\}$, $x_i \in \mathbb{R}^{D_1}$ with labels $\{l_1^x, l_2^x, \ldots, l_m^x\}$. The Euclidean data of videos are represented by $Y = \{y_1, y_2, \ldots, y_n\}, y_j \in \mathbb{R}^{D_2}$, with labels $\{l_1^y, l_2^y, \ldots, l_n^y\}$, while their Riemannian data are $Z = \{z_1, z_2, \ldots, z_n\}, z_j \in \mathcal{M}$ sharing the labels with their Euclidean data. In the following, we describe the components of the proposed CERML framework for this task.

Distance Metric. The distance metric Eq. (2) in Section 3.1 is instantiated for V2S/S2V face recognition as

$$d(x_i, y_j) + d(x_i, z_j) \\ = \sqrt{(W_x^T K_{x.i} - W_y^T K_{y.j})^T (W_x^T K_{x.i} - W_y^T K_{y.j})} \\ + \sqrt{(W_x^T K_{x.i} - W_z^T K_{z.j})^T (W_x^T K_{x.i} - W_z^T K_{z.j})}. \quad (26)$$

Objective Function. The objective function Eq. (10) in Section 3.2 takes the form

$$\min_{W_x, W_y, W_z} J(W_x, W_y, W_z) \\ = \min_{W_x, W_y, W_z} \{D(W_x, W_y, W_z) + \lambda_1 G(W_x, W_y, W_z) \\ + \lambda_2 T(W_x, W_y, W_z)\}, \quad (27)$$

where the distance constraint $D(W_x, W_y, W_z) = D(W_x, W_y) + D(W_x, W_z)$, the geometry constraint $G(W_x, W_y, W_z) = G_x(W_x) + G_y(W_y) + G_z(W_z)$, the transformation constraint $T(W_x, W_y, W_z) = \frac{1}{2}(\|W_x^T K_X\|_{\mathcal{F}}^2 + \|W_y^T K_Y\|_{\mathcal{F}}^2 + \|W_z^T K_Z\|_{\mathcal{F}}^2)$.

Initialization. In the initialization function Eq. (22), the optimization algorithm in Section 3.3 is instantiated with the matrix M^b, M^w as

$$M^b = \begin{bmatrix} K_x R_x^b K_x^T & -K_x A_{xy}^b K_y^T & -K_x A_{xz}^b K_z^T \\ -K_y (A_{xy}^b)^T K_x^T & K_y R_y^b K_y^T & 0 \\ -K_z (A_{xz}^b)^T K_x^T & 0 & K_z R_z^b K_z^T \end{bmatrix}, \quad (28)$$

$$M^w = \begin{bmatrix} K_x R_x^w K_x^T & -K_x A_{xy}^w K_y^T & -K_x A_{xz}^w K_z^T \\ -K_y (A_{xy}^w)^T K_x^T & K_y R_y^w K_y^T & 0 \\ -K_z (A_{xz}^w)^T K_x^T & 0 & K_z R_z^w K_z^T \end{bmatrix}. \quad (29)$$

Alternately Updating. The analytical solutions Eqs. (24) and (25) in the Section 3.3 can be rewritten as

$$W_x = (K_x(2B_x' + 2\lambda_1 L_x + 2\lambda_2 I)K_x^T)^{-1} \\ (K_x A_{xy} K_y^T W_y + K_x A_{xz} K_z^T W_z), \\ W_y = (K_y(B_y' + 2\lambda_1 L_y + 2\lambda_2 I)K_y^T)^{-1} K_y A_{xy} K_x^T W_x, \\ W_z = (K_z(B_z' + 2\lambda_1 L_z + 2\lambda_2 I)K_z^T)^{-1} K_z A_{xz} K_x^T W_x. \quad (30)$$

4.2 V2V Face Recognition

Similar to the case of V2S/S2V face recognition, each facial video sequence is commonly represented by the appearance mean of its frames and their pattern variation. Therefore, the task of V2V face recognition can be expressed as the problem of fusing the Euclidean data (i.e., feature mean) and the Riemannian representation (i.e., feature variation such as linear subspace) of video sequences of faces. Formally, the Euclidean data of videos are represented by $Y = \{y_1, y_2, \ldots, y_n\}, y_j \in \mathbb{R}^{D_2}$, with labels $\{l_1^y, l_2^y, \ldots, l_n^y\}$, while the Riemannian representations of such videos are $Z = \{z_1, z_2, \ldots, z_n\}, z_j \in \mathcal{M}$ sharing the labels with the Euclidean data. To adapt the proposed CERML framework to this task, we now define its components.

Distance Metric. The distance metrics Eqs. (3) and (4) in Section 3.1 are implemented for V2V face recognition as

$$d(y_i, y_j) + d(z_i, z_j) \\ = \sqrt{(W_y^T K_{y.i} - W_y^T K_{y.j})^T (W_y^T K_{y.i} - W_y^T K_{y.j})} \\ + \sqrt{(W_z^T K_{z.i} - W_z^T K_{z.j})^T (W_z^T K_{z.i} - W_z^T K_{z.j})}. \quad (31)$$

Objective Function. The objective function Eq. (10) in Section 3.2 is instantiated as

$$\min_{W_y, W_z} J(W_y, W_z) \\ = \min_{W_y, W_z} \{D(W_y, W_z) + \lambda_1 G(W_y, W_z) + \lambda_2 T(W_y, W_z)\}, \quad (32)$$

where the distance constraint $D(W_y, W_z) = D(W_y) + D(W_z)$, the geometry constraint $G(W_y, W_z) = G_y(W_y) + G_z(W_z)$, the transformation constraint $T(W_y, W_z) = \frac{1}{2}(\|W_y^T K_Y\|_{\mathcal{F}}^2 + \|W_z^T K_Z\|_{\mathcal{F}}^2)$.

Initialization. The initialized objective function Eq. (22) in the optimization algorithm in Section 3.3 is instantiated by defining the matrix M^b, M^w as

$$M^b = \begin{bmatrix} K_y R_y^b K_y^T & -K_y A^b K_z^T \\ -K_z(A^b)^T K_y^T & K_z R_z^b K_z^T \end{bmatrix}, \tag{33}$$

$$M^w = \begin{bmatrix} K_y R_y^w K_y^T & -K_y A^w K_z^T \\ -K_z(A^w)^T K_y^T & K_z R_z^w K_z^T \end{bmatrix}. \tag{34}$$

Alternately Updating. The analytical solutions Eqs. (24) and (25) in Section 3.3 can be derived as

$$W_y = (K_y(B_y' + 2\lambda_1 L_y + 2\lambda_2 I)K_y^T)^{-1} K_y A K_z^T W_z,$$
$$W_z = (K_z(B_z' + 2\lambda_1 L_z + 2\lambda_2 I)K_z^T)^{-1} K_z A K_y^T W_y. \tag{35}$$

5 EXPERIMENTAL EVALUATION

We conduct evaluations for three video-based face recognition tasks being—Video-to-Still, Still-to-Video and Video-to-Video face recognition—on four challenging video face databases. These databases are YouTube Celebrities (YTC) [52], YouTube Face DB (YTF) [53], Point-and-Shoot Challenge (PaSC) [54] and COX face [55].

The YTC [52] and YTF [53] are both popular internet video face datasets collecting from YouTube. The YTC contains 1,910 video clips of 47 celebrities. The video frames often exhibit a large variation of pose and illumination, as well as degradations such as compression effects (see Fig. 3a). The YTF, contains 3,425 videos of 1,595 persons. As shown in Fig. 3b, there are again large variations in pose, illumination, and expression. Thus, the YTF is very challenging for verifying faces from these internet videos.

The PaSC [54] and COX [55] are designed to simulate more of a video surveillance system. The PaSC [54] was collected for face recognition from stills and videos captured by point-and-shoot cameras. It includes 9,376 still images and 2,802 videos of 293 people in total. The data has large variation in terms of distance to the camera, alternative sensors, frontal versus not-frontal views, and varying location (see Fig. 3c) The COX captures 3,000 videos and 1,000 still images of 1,000 different persons with 3 different camcorders located in different positions. As shown in Fig. 3d, most of the video frames are of low resolution and low quality, with blur, and captured under poor lighting.

5.1 V2S/S2V Face Recognition
V2S and S2V face recognition matches still face images against video sequences of faces. To evaluate our proposed method in such two face recognition scenarios, we employ two standard video face databases: PaSC [54] and COX [55].

5.1.1 Dataset Setting
On the PaSC, the facial region is cropped by using the eye coordinates from [54]. Then the cropped facial region is aligned and scaled to a size of 224×224 pixels. Following [4], [10], [56], we use the approach of [15] to extract deep face
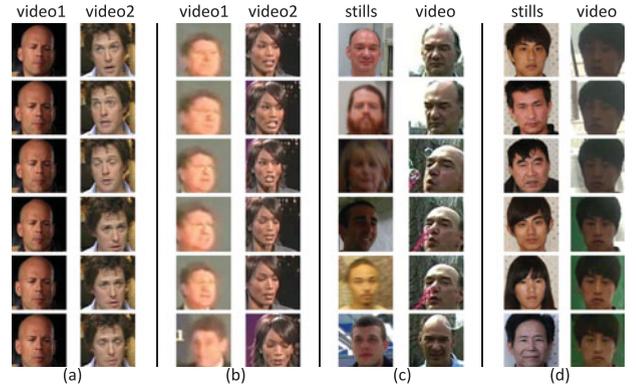

Fig. 3. Example still images and video frames from internet face datasets YTC (a), YTF (b) and surveillance-like face datasets PaSC (c), COX (d).

features from the normalized face images. For V2S face verification, the target set includes 9,376 images of 293 people while the query set contains 2,802 videos of 265 people. Since the videos are grouped into the sets of control and handheld videos respectively, the V2S evaluation on the PaSC consists of two tests: Video (control)-Still and Video (handheld)-Still.

For the COX database, we use the face detection and the positions of the eyes provided by the work in [55]. In the scenario of V2S/S2V face recognition, we implement two types of feature extractions. In the first setting, we first normalize face images with a size of 48×60, and then use resulting gray-scale pixel values as gray feature vectors. In the other setting, as done on the PaSC, we also extract deep face features by the approach of [15]. In the V2S evaluation, the target set contains still images of the persons with known identities, while the query samples are video clips of faces to be recognized. In contrast, the target set of the S2V scenario conversely contains videos of faces while the queries are still face images. There are 3 testing sets of videos, each of which contains 700 videos from 700 subjects. Therefore, in total 6 tests (i.e., V1-S, V2-S, V3-S, S-V1, S-V2, S-V3, where Vi is the ith video testing set) are conducted.

5.1.2 Method Setting
In the evaluation of V2S/S2V face recognition, besides to the deep learning method VGGDeepFace [15] that reported the state of the art on YTF, we also compare two groups of existing metric learning methods as listed below. The homogeneous (Euclidean) metric learning approaches learn the single-view metric between Euclidean features of video frames/still images, and adopt the maximal pooling on the matching between images and frames within one video. The heterogeneous metric learning methods learn the cross-view metric among the Riemannian representations[1] of videos, their Euclidean features and the Euclidean features of still images. As KPLS, KCCA and KGMA are all both designed to analyze heterogeneous data, we feed them with our proposed Euclidean-to-Grassmannian (EG), Euclidean-to-AffineGrassmannian (EA) and Euclidean-to-SPD (ES) heterogeneous data, which are also the inputs of our CERML.

---

1. For the SPD matrix representation, we compute a covariance matrix for each set of face features that belong to the same video clip. Regarding linear subspace, we applied eigen-decomposition on each resulting covariance matrix to obtain an orthonormal basis matrix as the representation. Further, we combine mean vector and linear subspace together to represent affine subspace.

TABLE 1
V2S/S2V Face Recognition Results (%) on PaSC and COX Using Gray/Deep Features

Methods	PaSC (deep)		COX (gray/deep)					
	V(con)-S	V(han)-S	V1-S	V2-S	V3-S	S-V1	S-V2	S-V3
VGGDeepFace [15]	68.62	65.29	−/79.10	−/77.53	−/79.03	−/59.31	−/65.21	−/74.29
NCA [21]	68.91	67.48	39.14/79.83	31.57/74.21	57.57/80.69	37.71/72.01	32.14/69.39	58.86/79.51
ITML [22]	67.25	65.33	19.83/82.43	18.20/73.49	36.63/86.53	26.66/73.03	25.21/61.57	47.57/82.29
LFDA [23]	**72.44**	**69.86**	21.41/66.58	22.17/55.29	43.99/72.86	40.54/78.25	33.90/68.14	61.40/84.15
LMNN [24]	71.12	67.12	34.44/83.25	30.03/72.19	58.06/83.25	37.84/76.12	35.77/70.26	63.33/80.92
PSDML [25]	66.15	63.61	12.14/65.09	9.43/58.16	25.43/80.05	7.04/54.15	4.14/49.16	29.86/78.57
KPLS [28]-EG	42.29	41.21	21.83/46.19	18.50/44.90	30.89/44.67	15.01/49.77	12.41/50.31	25.63/55.07
KPLS [28]-EA	44.42	42.30	21.54/47.31	19.19/46.94	29.41/37.96	15.73/45.97	12.51/47.10	24.54/41.41
KPLS [28]-ES	44.27	42.08	20.21/46.26	16.21/45.16	27.23/42.16	14.83/46.21	11.61/46.21	23.99/43.63
KCCA [26]-EG	58.08	55.71	32.51/73.53	28.87/70.94	48.43/78.79	30.16/73.03	27.34/70.60	44.91/78.59
KCCA [26]-EA	61.87	60.58	30.33/75.03	28.39/72.34	47.74/75.94	28.49/74.63	26.49/72.26	45.21/74.79
KCCA [26]-ES	61.36	60.11	38.60/80.87	33.20/76.63	53.26/81.94	36.39/80.00	30.87/76.76	50.96/81.40
KGMA [31]-EG	60.05	58.18	32.41/75.24	28.96/72.91	48.37/79.93	30.06/75.19	27.57/72.57	44.99/80.06
KGMA [31]-EA	64.87	63.58	30.60/79.33	28.34/76.19	47.74/79.94	28.54/78.63	26.20/76.06	45.27/78.54
KGMA [31]-ES	63.76	62.32	41.89/80.91	38.29/76.53	52.87/81.90	38.03/80.00	33.29/76.69	50.06/81.41
CERML-EG	63.34	60.92	32.63/85.71	33.89/82.51	49.33/**87.23**	43.29/88.80	41.19/85.69	58.71/**90.99**
CERML-EA	67.95	66.16	38.77/**86.40**	37.57/**83.13**	53.93/86.76	43.93/**88.97**	41.56/**85.84**	57.34/90.26
CERML-ES	70.64	68.91	51.41/86.21	49.81/82.66	64.01/86.64	52.39/88.93	49.39/85.37	65.19/89.64

Here EG, EA and ES represent Euclidean-to-Grassmannian, Euclidean-to-AffineGrassmannian and Euclidean-to-SPD matching cases, respectively. Con and han mean the control and handheld settings.

(1) Homogeneous (Euclidean) metric learning methods: Neighborhood Components Analysis (NCA) [21], Information-Theoretic Metric Learning (ITML) [22], Local Fisher Discriminant Analysis (LFDA) [23], Large Margin Nearest Neighbor (LMNN) [24] and Point-to-Set Distance Metric Learning (PSDML) [25];

(2) Heterogeneous metric learning methods: Kernel Partial Least Squares (KPLS) [28], Kernel Canonical Correlation Analysis (KCCA) [26] and Kernel Generalized Multiview Linear Discriminant Analysis (KGMA) [31].

For fair comparison, we tune the key parameters of the comparative methods according to the suggestions from the original works. For NCA, the maximum number of line searches is set to 5. For ITML, the lower/upper bound distance is set to the mean distance minus/plus standard variance, and its other parameters are set to the default values designed in its released code. In LFDA, the neighborhood number k is set to 7. For LMNN, the number of neighborhood is set to 5, the maximum iteration number is set to 500, the portion of training samples in validation is 30 percent. For PSDML, we set the regularization parameter as $\kappa = 0.8$, the number of negative pairs per sample $k = 6$. For KPLS and KGMA, the numbers of the factors are set with the class number of training data. For the proposed method CERML, we set the parameters $\lambda_1 = 0.01, \lambda_2 = 0.1$, the neighborhood number $k_1 = 1, k_2 = 20$, the kernel widths σs are all specified from the mean distances respectively on the training multi-view data, and the number of iterations is set to 20. As studied in our previous work [20], we find that adding the cross-view kernels (see the supplementary material for their definitions, available online) into the original single-view kernels does improve the V2S/S2V face recognition. Thus, we use the proposed cross-view kernels in [20] to concatenate the EG/EA/ES kernels for CERML. For the comparisons between single-view and cross-view kernel cases, readers are referred to the supplementary material, available online.

5.1.3 Results and Analysis

We summarize the V2S/S2V face recognition results on the PaSC and COX databases in Table 1, where each reported result on COX is the mean rank-1 identification rate over ten random runs of testing, while the presented results on PaSC are rank-1 verification rates at a false acceptance rate (FAR) = 0.01. In addition, we present comparisons in terms of running time in the supplementary material, available online.

As shown in Table 1, we can achieve some observations. On PaSC, the homogeneous (Euclidean) metric learning methods generally outperform the existing heterogeneous metric learning methods. This is because the facial videos in the PaSC dataset are typically taken under very large variations in head pose, lighting, and locations. Hence, it is difficult for them to use a single type of representation to encode the video features. Moreover, it is also non-trivial to learn a correlation model between such highly heterogeneous image features and video features. In contrast, by exploiting multiple features for video representations and designing a more sophisticated heterogeneous metric learning scheme, our proposed CERML can achieve comparable results with the state-of-the-art. On COX, in most of tests, the exiting heterogeneous metric learning methods KCCA and KGMA coupled with our proposed heterogeneous data model are comparable with state-of-the-art homogeneous metric learning. In contrast, in the two tests of V3-S and S-V3, since the videos typically record more frontal face images with little variations, KCCA and KGMA cannot take advantage of the variation modeling on videos and thus are outperformed by the Euclidean metric learning methods. In spite of this challenge, the proposed CERML achieves state-of-the-art results on all the COX tests. Especially, coupling with deep features, the improvements of CERML over the existing state-of-the-art methods LMNN and KGMA are around 9 and 7 percent, respectively, on average. By comparing the deep learning method VGGDeepFace on COX and PaSC, we find that the
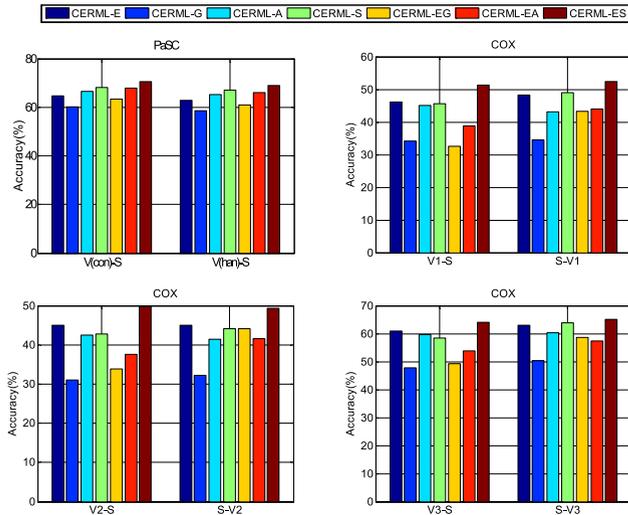
Fig. 4. V2S/S2V face recognition results (%) of the proposed CEMRL dealing with different representations of videos for PaSC (deep feature) and COX (gray feature). Here, CERML-E, CERML-G, CERML-A, CERML-S, CERML-EG, CERML-EA, CERML-ES respectively indicate videos are represented by mean, subspace, affine subspace, SPD matrix, mean+subspace, mean+affine subspace, mean+SPD matrix. *Note that CERML-G/A/S is the proposed method in our prior work [21].*

CERML consistently makes big improvements (about 10 percent on average) when using deep features. This verifies the proposed first- and second-order pooling scheme can improve V2S/S2V face recognition.

Besides, we also present the performances of our CERML with different video models working on PaSC (deep feature) and COX (gray feature) in Fig. 4. We find that jointly exploiting the first-order pooling (i.e., mean) and the second-order pooling (i.e., linear subspace, affine subspace, covariance matrix) often significantly beats their separate exploitation, which was studied in our prior work [20]. This further validates the effectiveness of the extended CERML method.

In Fig. 5 we also report the convergence characteristics of the optimization algorithm of the proposed CERML-ES for V2S/S2V face recognition on COX. As shown in Fig. 5, the objective function Eq. (27) of the proposed CERML is able to converge to a stable and desirable solution after about 20 iterations. In general, the objective function values will decrease mildly when we add more iterations to run the proposed optimization algorithm. Empirically, in most of evaluations, we found the resulting accuracies of running about 20 iterations are generally a bit higher than those of performing more iterations. Besides, its also worth mentioning that fixing the iteration number in all evaluations can also show our methods insensitivity to the parameter setting to some extent. The good convergence mainly attributes to the well-designed initialization strategy (i.e., an initialization with the well-studied Fisher criterion) and the alternate updating on the parameter transformation matrices. In other words, adopting a good initialization strategy and regularizing the change in the transformation matrices will help to avoid the failure of convergence.

5.2 V2V Face Recognition

V2V face recognition queries a video against a set of target videos. To evaluate the proposed method, we use four face datasets, i.e., YTC [52], YTF [53], PaSC [54] and COX [55].
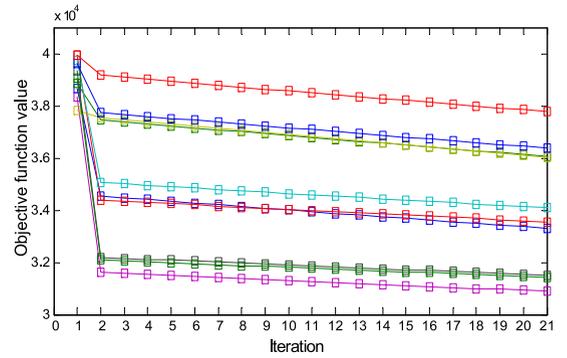

Fig. 5. Convergence characteristics of the optimization algorithm of the proposed CERML-ES in the task of V2S face recognition on COX. Here, the 10 lines indicate the results of the 10 random V1-S testings on COX. The value '1' in x-axis is the case of the initialization.

5.2.1 Dataset Setting

For the YTC dataset, we resized each face image to a 20×20 image as was also done in [2], [18], and pre-processed the resulting image with histogram equalization to eliminate lighting effects. As done in the last evaluation, we extract both gray features (pixel values) and deeply learned features with VGGDeepFace [15] from each face image. Following the prior works [2], [18], [57], [58], we conduct tenfold cross validation experiments, i.e., 10 randomly selected gallery/probe combinations. In each fold, one person has 3 randomly chosen videos for the gallery and 6 for probes.

By employing the provided data of the YTF, we directly crop and normalize the face images from videos, and extract both pixel-valued gray features and deep features from the normalized face images. For this database, we follow the standard evaluation protocol [53] to perform standard, tenfold, cross validation, V2V face identification tests. Specifically, we utilize the officially provided 5,000 video pairs, which are equally divided into 10 folds. Each fold contains 250 intra-personal pairs and 250 inter-personal pairs.

For the PaSC, according to the metadata from [54], we crop each facial image to a color one of size 224×224. Similar to the V2S evaluation on PaSC, we employ [15] to extract deep face features on the normalized faces. For the V2V evaluation, there are two video face verification tests: control-to-control and handheld-to-handheld. In both of them, the target and query sigsets contain the same set of videos. Since the same 1,401 control/handheld videos serve as both the target and query sets, the 'same video' comparisons are excluded.

For V2V identification, the COX has 3 videos per subject respectively from 3 camcorders, which generates 6 testings. The 10 random partitions of the 300/700 subjects are designed for training and testing. In the V2V face recognition testing, each video face frame is normalized to a grayscale image. Similar to its V2S/S2V evaluation, we not only extract pixel-valued gray features, but also use deep features with the deep learning method of VGGDeepFace [15].

5.2.2 Method Setting

In this evaluation, we compare the proposed CERML with three state-the-art deep learning methods being DeepFace [13], FaceNet [14], VGGDeepFace [15] and DisDeepFace [17]. Besides, we also study groups of state-of-the-art Riemannian metric learning methods. The first category of methods first model videos with linear subspaces lying on a

TABLE 2
V2V Face Recognition Results (%) on YTC and
YTF Using Gray/Deep Features

Methods	YTC (gray/deep)	YTF (gray/deep)
DeepFace [13]	–/–	–/91.4
FaceNet [14]	–/–	–/**95.1**
VGGDeepFace [15]	–/83.74	–/91.78
DisDeepFace [17]	–/–	–/94.9
DCC [59]	68.85/86.15	68.28/92.52
GDA [8]	65.02/86.44	67.00/89.20
GGDA [39]	66.56/86.54	66.56/91.60
PML [10]	66.69/86.98	67.30/92.58
AHISD [60]	66.37/81.49	64.80/90.74
CHISD [60]	66.62/74.88	66.30/90.00
SSDML [25]	68.85/85.59	65.38/88.26
CDL [2]	69.72/85.98	64.94/90.65
LMKML [18]	68.13/85.16	64.39/89.53
CERML-EG	68.08/87.62	69.42/93.36
CERML-EA	69.57/88.01	68.89/94.06
CERML-ES	**72.38**/**88.51**	68.36/93.44

Here EG, EA and ES are the Euclidean-to-Grassmannian, Euclidean-to-AffineGrassmannian and Euclidean-to-SPD matchings.

Grassmann manifold and then learn a Grassmannian metric for comparing linear subspaces. The second group of methods first represents videos with affine subspaces residing on an Affine Grassmann manifold and then compute/learn the Riemannian metric for matching affine subspaces. The third kind of methods first employs SPD matrices to represent videos and learns a Riemannian metric on the SPD manifold for comparing SPD data.

(1) Grassmannian metric learning methods: Discriminative Canonical Correlations (DCC) [59], Grassmann Discriminant Analysis (GDA) [8], Grassmannian Graph-Embedding Discriminant Analysis (GGDA) [39], Projection Metric Learning (PML) [10];

(2) Affine Grassmannian computing/metric learning methods: Affine Hull based Image Set Distance (AHISD) [60], Convex Hull based Image Set Distance (CHISD) [60], Set-to-Set Distance Metric Learning (SSDML) [25];

(3) SPD Riemannian metric learning methods: Localized Multi-Kernel Metric Learning (LMKML) [18], Covariance Discriminative Learning (CDL) [2].

In order to achieve a fair comparison, the key parameters of each method are empirically tuned according to the recommendations in the original works. For MSM/AHISD, the first canonical correlation or leading component is exploited when comparing two subspaces. For the first group of methods DCC/GDA/GGDA, the dimensionality of the resulting discriminant subspace is tuned from 1 to 10. For GDA/GGDA, the final dimensionality is set to $c-1$ (c is the number of face classes in training). For AHISD, the leading component is exploited when comparing affine subspaces. For SSDML, its key parameters are tuned and empirically set as: $\lambda_1 = 0.001, \lambda_2 = 0.5$, the numbers of positive and negative pairs per sample are 10 and 20 respectively. In GGDA, the combination parameter β is tuned around the value of 100. For LMKML, the widths of Gaussian kernels are tuned around the mean distance. For our CERML, similar to the V2S/S2V evaluation, the regularization parameters are set as $\lambda_1 = 0.01, \lambda_2 = 0.1$, the neighborhood number $k_1 = 1$, $k_2 = 20$, the kernel widths σs are equal to the mean distances on the training multi-view data, and the number of iterations is set to 20.

5.2.3 Results and Analysis

The V2V face recognition tests on the four video face databases are summarized in Tables 2 and 3, where each accuracy on YTC and COX is the mean rank-1 identification rate over ten random runs of testing, while the results on YTF and PaSC are mean verification rates and rank-1 verification rates at FAR = 0.01, respectively. Besides, the running time of the competing methods are also presented in the supplementary material, available online.

From the results on the internet video face databases YTC and YTF in Table 2, it can be observed that the three existing types of Riemannian metric learning achieve comparable V2V face recognition accuracies. This demonstrates that the Riemannian representations, i.e., linear subspace and SPD matrix, employed by such Riemannian metric learning

TABLE 3
V2V Face Recognition Results (%) on PaSC and COX Using Gray/Deep Features

Methods	PaSC (deep)		COX (gray/deep)					
	V(con)-V(con)	V(han)-V(han)	V2-V1	V3-V1	V3-V2	V1-V2	V1-V3	V2-V3
VGGDeepFace[15]	78.82	68.24	–/92.24	–/87.54	–/91.63	–/92.34	–/92.47	–/95.96
DCC [59]	75.83	67.04	62.53/95.86	66.10/95.57	50.56/93.00	56.09/94.29	53.84/96.86	45.19/96.29
GDA [8]	71.38	67.49	68.61/95.11	77.70/95.87	71.59/95.16	65.93/94.41	76.11/96.10	74.83/96.26
GGDA [39]	66.71	68.41	70.80/95.81	76.23/96.30	71.99/95.61	69.17/95.34	76.77/96.66	77.43/96.61
PML [10]	73.45	68.32	71.27/95.57	78.91/95.43	73.24/93.29	64.62/95.86	78.26/97.13	78.15/97.00
AHISD [60]	53.93	45.11	53.03/92.85	36.13/95.57	17.50/95.43	43.51/93.57	34.99/92.43	18.80/94.71
CHISD [60]	60.54	47.00	56.90/92.43	30.13/94.57	15.03/93.43	44.36/91.57	26.40/94.06	13.69/94.57
SSDML [25]	65.32	56.23	60.13/77.43	53.14/90.71	28.73/89.57	47.91/70.43	44.42/85.43	27.34/87.57
CDL [2]	72.69	65.44	78.43/95.53	85.31/97.61	79.71/96.40	75.56/95.96	85.84/97.33	81.87/96.51
LMKML [18]	70.41	66.15	56.14/94.73	44.26/95.16	33.14/96.37	55.37/93.81	39.83/96.12	29.54/96.28
CERML-EG	**80.11**	**77.37**	87.59/97.77	92.41/98.07	88.54/97.39	83.21/97.66	92.09/**98.59**	91.16/**97.77**
CERML-EA	77.71	75.03	87.14/**98.26**	91.94/**98.33**	88.30/**97.60**	82.81/**97.97**	92.03/98.49	91.16/97.66
CERML-ES	79.92	76.92	90.31/98.17	94.83/98.27	91.51/97.46	87.06/97.71	95.13/98.31	93.89/97.64

Here EG, EA and ES indicate Euclidean-to-Grassmannian, Euclidean-to-AffineGrassmannian and Euclidean-to-SPD matching, respectively. Con and han represent the control and handheld settings.
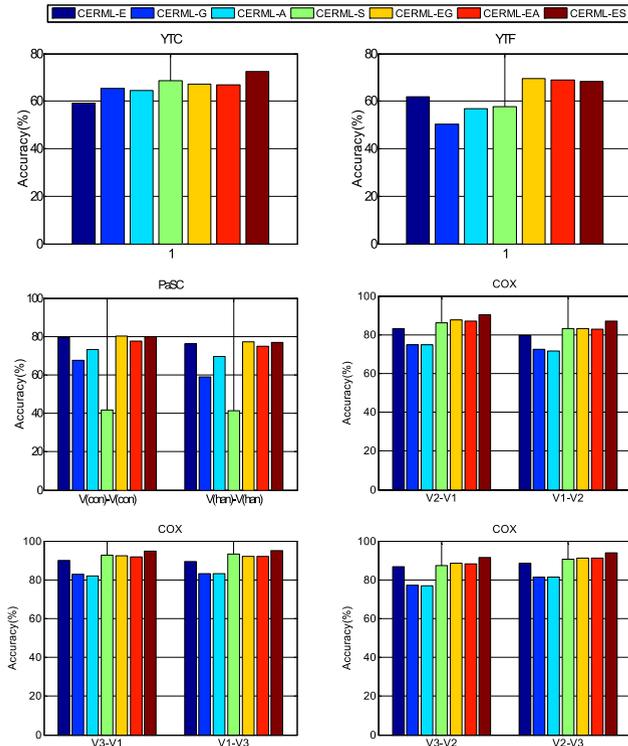
Fig. 6. V2V face recognition results (%) of the proposed CEMRL dealing with different representations of videos using gray features for YTC, YTF, COX and deep features for PaSC. Here, CERML-E, CERML-G, CERML-A, CERML-S, CERML-EG, CERML-EA, CERML-ES respectively indicate videos are represented by mean, subspace, affine subspace, SPD matrix, mean+subspace, mean+affine subspace, mean+SPD matrix.
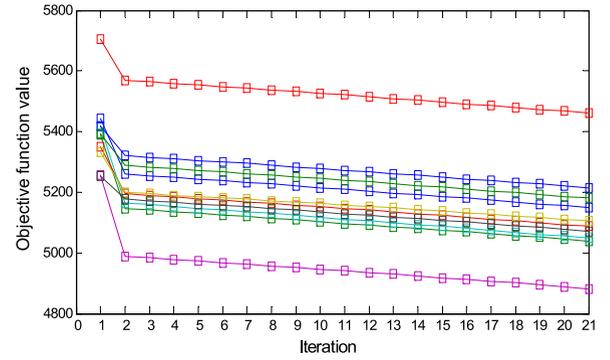

Fig. 7. Convergence behaviors of the optimization algorithm of the proposed CERML-ES in the task of V2V face recognition for COX. Here, the 10 lines respectively indicate the results of the 10 random V2-V1 tests on COX. The value '1' along the x-axis is the case of the initialization.

methods typically encode approximately the same information in terms of variations of videos for video-based face recognition. In contrast, the proposed CERML simultaneously exploits the mean and the variation, resulting in more robust face recognition. Hence, CERML generally outperform all the competing methods on the two databases. In addition, by studying the behavior of the state-of-the deep learning methods, we observe that our CERML can be comparable with or even surpass them.

The evaluations on the two surveillance-like video face databases PaSC and COX are reported in Table 3. Approximately the same conclusions can be drawn from the results on the two datasets. On PaSC, the three affine Grassmannian learning methods are generally outperformed by the other two kinds of Riemannian metric learning methods. This may be because AHISD and CHISD exploit the appropriate distance metric between Riemannian representations without employing the label information of the training data. Besides, SSDML just treats each video with an affine combination of frames without considering its Riemannian structure, and thus yields worse performances on PaSC. By fusing the mean and the variation information on videos, our CERML-EG performs the best with improvements of about 4 and 10 percent over the state-of-the-art method DCC in the two tests on PaSC, respectively. On COX, lower performances are also achieved by the three affine Grassmannian metric learning methods for the same reasons mentioned above. Compared with the existing Riemannian metric learning methods, the proposed CERML can achieve the state-of-the-art in all the V2V face recognition tests on COX. Specifically, whenever

using gray features or deep features, CERML always reaches some improvements over the existing state-of-the-art metric learning methods. Furthermore, we find that the proposed CERML with deep features has an average gain of 5 percent over the state-of-the-art deep learning method VGGDeepFace on the PaSC and COX databases.

In addition, we also report the performances of our CERML with different video models working on YTC, YTF, PaSC and COX in Fig. 6. As can be seen, simultaneously exploiting the mean appearance and pattern variance typically performs better than exploiting them separately. This further demonstrates the effectiveness of fusing Euclidean and Riemannian representations in the proposed metric learning scheme in our CERML.

In the end, we present the convergence behavior of the optimization algorithm of the proposed CERML-ES in the scenario of V2V face recognition on COX (see Fig. 7). As seen, the objective function Eq. (32) of the algorithm can converge to a desirable value after tens of iterations.

6   CONCLUSION AND FUTURE WORK

In this paper, we have introduced a novel heterogeneous metric learning framework that works across a Euclidean space and a Riemannian manifold to match/fuse Euclidean and Riemannian representations of videos. The proposed method offers a unified framework for three typical tasks of video-based face recognition. Our extensive experimental evaluations have clearly shown that the new technique can achieve the state-of-the-art on four challenging video face datasets in the three video-based face recognition tasks.

Our work contributes to learn a cross-view metric from a Euclidean space to a Riemannian manifold, by exploiting the Riemannian metric learning scheme of kernel embedding which introduces several intrinsic drawbacks (e.g., undesirable scalability) of traditional kernel learning methods as well. For future work, studying how to improve the proposed framework with other more effective Riemannian metric learning schemes such as manifold-to-manifold embedding would be very interesting.

REFERENCES

[1] J. Hamm and D. D. Lee, "Extended Grassmann kernels for sub-space-based learning," in *Proc. Int. Conf. Neural Inf. Process. Syst.*, 2009, pp. 601–608.

[2] R. Wang, H. Guo, L. Davis, and Q. Dai, "Covariance discriminative learning: A natural and efficient approach to image set classification," in *Proc. IEEE Conf. Comput. Vis. Pattern Recognit.*, 2012, pp. 2496–2503.

[3] R. Vemulapalli, J. Pillai, and R. Chellappa, "Kernel learning for extrinsic classification of manifold features," in *Proc. IEEE Conf. Comput. Vis. Pattern Recognit.*, 2013, pp. 1782–1789.

[4] Z. Huang, R. Wang, S. Shan, and X. Chen, "Face recognition on large-scale video in the wild with hybrid Euclidean-and-Riemannian metric learning," *Pattern Recognit.*, vol. 48, pp. 3113–3124, 2015.

[5] W. Wang, R. Wang, Z. Huang, S. Shan, and X. Chen, "Discriminant analysis on Riemannian manifold of Gaussian distributions for face recognition with image sets," in *Proc. IEEE Conf. Comput. Vis. Pattern Recognit.*, 2015, pp. 2048–2057.

[6] S.-I. Amari and H. Nagaoka, *Methods of Information Geometry*. London, U.K.: Oxford Univ. Press, 2000.

[7] M. Lovrić, M. Min-Oo, and E. A. Ruh, "Multivariate normal distributions parametrized as a Riemannian symmetric space," *J. Multivariate Anal.*, vol. 74, pp. 36–48, 2000.

[8] J. Hamm and D. D. Lee, "Grassmann discriminant analysis: A unifying view on subspace-based learning," in *Proc. Int. Conf. Mach. Learn.*, 2008, pp. 376–383.

[9] K. Fukunaga, *Introduction to Statistical Pattern Recognition*. New York, NY, USA: Academic, 2013.

[10] Z. Huang, R. Wang, S. Shan, and X. Chen, "Projection metric learning on Grassmann manifold with application to video based face recognition," in *Proc. IEEE Conf. Comput. Vis. Pattern Recognit.*, 2015, pp. 140–149.

[11] H. Wold, "Partial least squares," *Encyclopedia of Statistical Sciences*, New York, NY, USA: Wiley, vol. 6, pp. 581–591, 1985.

[12] M. T. Harandi, M. Salzmann, and R. Hartley, "From manifold to manifold: Geometry-aware dimensionality reduction for SPD matrices," in *Proc. Eur. Conf. Comput. Vis.*, 2014, pp. 17–32.

[13] Y. Taigman, M. Yang, M. Ranzato, and L. Wolf, "DeepFace: Closing the gap to human-level performance in face verification," in *Proc. IEEE Conf. Comput. Vis. Pattern Recognit.*, 2014, pp. 1701–1708.

[14] F. Schroff, D. Kalenichenko, and J. Philbin, "FaceNet: A unified embedding for face recognition and clustering," in *Proc. IEEE Conf. Comput. Vis. Pattern Recognit.*, 2015, pp. 815–823.

[15] O. M. Parkhi, A. Vedaldi, and A. Zisserman, "Deep face recognition," in *Proc. Brit. Mach. Vis. Conf.*, 2015, pp. 1–12.

[16] Y. Sun, D. Liang, X. Wang, and X. Tang, "DeepID3: Face recognition with very deep neural networks," arXiv:1502.00873, 2015.

[17] Y. Wen, K. Zhang, Z. Li, and Y. Qiao, "A discriminative feature learning approach for deep face recognition," in *Proc. Eur. Conf. Comput. Vis.*, 2016, pp. 499–515.

[18] J. Lu, G. Wang, and P. Moulin, "Image set classification using holistic multiple order statistics features and localized multi-kernel metric learning," in *Proc. IEEE Int. Conf. Comput. Vis.*, 2013, pp. 329–336.

[19] M. Liu, R. Wang, S. Li, S. Shan, Z. Huang, and X. Chen, "Combining multiple kernel methods on Riemannian manifold for emotion recognition in the wild," in *Proc. ACM Int. Conf. Multimodel Interaction. Workshop*, 2014, pp. 494–501.

[20] Z. Huang, R. Wang, S. Shan, and X. Chen, "Learning Euclidean-to-Riemannian metric for point-to-set classification," in *Proc. IEEE Conf. Comput. Vis. Pattern Recognit.*, 2014, pp. 1677–1684.

[21] J. Goldberger, S. Roweis, G. Hinton, and R. Salakhutdinov, "Neighbourhood components analysis," in *Proc. Int. Conf. Neural Inf. Process. Syst.*, 2004, pp. 513–520.

[22] J. V. Davis, B. Kulis, P. Jain, S. Sra, and I. S. Dhillon, "Information-theoretic metric learning," in *Proc. Int. Conf. Mach. Learn.*, 2007, pp. 209–216.

[23] M. Sugiyama, "Dimensionality reduction of multimodal labeled data by local Fisher discriminant analysis," *J. Mach. Learn. Res.*, vol. 8, pp. 1027–1061, 2007.

[24] K. Q. Weinberger and L. K. Saul, "Distance metric learning for large margin nearest neighbor classification," *J. Mach. Learn. Res.*, vol. 10, pp. 207–244, 2009.

[25] P. Zhu, L. Zhang, W. Zuo, and D. Zhang, "From point to set: Extend the learning of distance metrics," in *Proc. IEEE Int. Conf. Comput. Vis.*, 2013, pp. 2664–2671.

[26] D. Hardoon, S. Szedmak, and J. Shawe-Taylor, "Canonical correlation analysis: An overview with application to learning methods," *Neural Comput.*, vol. 16, no. 12, pp. 2639–2664, Dec. 2004.

[27] M. M. Bronstein, A. M. Bronstein, F. Michel, and N. Paragios, "Data fusion through cross-modality metric learning using similarity-sensitive hashing," in *Proc. IEEE Comput. Soc. Conf. Comput. Vis. Pattern Recognit.*, 2010, pp. 3594–3601.

[28] A. Sharma and D. Jacobs, "Bypassing synthesis: PLS for face recognition with pose, low-resolution and sketch," in *Proc. IEEE Conf. Comput. Vis. Pattern Recognit.*, 2011, pp. 593–600.

[29] N. Quadrianto and C. H. Lampert, "Learning multi-view neighborhood preserving projections," in *Proc. Int. Conf. Mach. Learn.*, 2011, pp. 425–432.

[30] B. McFee and G. Lanckriet, "Learning multi-modal similarity," *J. Mach. Learn. Res.*, vol. 12, pp. 491–523, 2011.

[31] A. Sharma, A. Kumar, H. Daume, and D. Jacobs, "Generalized multiview analysis: A discriminative latent space," in *Proc. IEEE Conf. Comput. Vis. Pattern Recognit.*, 2012, pp. 2160–2167.

[32] X. Zhai, Y. Peng, and J. Xiao, "Heterogeneous metric learning with joint graph regularization for cross-media retrieval," in *Proc. 27th AAAI Conf. Artif. Intell.*, 2013, pp. 1198–1204.

[33] O. Tuzel, F. Porikli, and P. Meer, "Pedestrian detection via classification on Riemannian manifolds," *IEEE Trans. Pattern Anal. Mach. Intell.*, vol. 30, no. 10, pp. 1713–1727, Oct. 2008.

[34] D. Tosato, M. Farenzena, M. Cristani, M. Spera, and V. Murino, "Multi-class classification on Riemannian manifolds for video surveillance," in *Proc. Eur. Conf. Comput. Vis.*, 2010, pp. 378–391.

[35] P. Turaga, A. Veeraraghavan, A. Srivastava, and R. Chellappa, "Statistical computations on Grassmann and Stiefel manifolds for image and video-based recognition," *IEEE Trans. Pattern Anal. Mach. Intell.*, vol. 33, no. 11, pp. 2273–2286, Nov. 2011.

[36] J. Carreira, R. Caseiro, J. Caseiro, and C. Sminchisescu, "Semantic segmentation with second-order pooling," in *Proc. Eur. Conf. Comput. Vis.*, 2012, pp. 430–443.

[37] A. Sanin, C. Sanderson, M. T. Harandi, and B. C. Lovell, "Spatio-temporal covariance descriptors for action and gesture recognition," in *Proc. Winter Conf. Appl. Comput. Vis. Workshop*, 2013, pp. 103–110.

[38] C. Xu, C. Lu, J. Gao, W. Zheng, T. Wang, and S. Yan, "Discriminative analysis for symmetric positive definite matrices on lie groups," *IEEE Trans. Circuits Syst. Video Technol.*, vol. 25, no. 10, pp. 1576–1585, Oct. 2015.

[39] M. T. Harandi, C. Sanderson, S. Shirazi, and B. C. Lovell, "Graph embedding discriminant analysis on Grassmannian manifolds for improved image set matching," in *Proc. IEEE Conf. Comput. Vis. Pattern Recognit.*, 2011, pp. 2705–2712.

[40] P. Li, Q. Wang, W. Zuo, and L. Zhang, "Log-Euclidean kernels for sparse representation and dictionary learning," in *Proc. IEEE Int. Conf. Comput. Vis.*, 2013, pp. 1601–1608.

[41] H. Minh, M. Biagio, and V. Murino, "Log-Hilbert-Schmidt metric between positive definite operators on Hilbert spaces," in *Proc. Int. Conf. Neural Inf. Process. Syst.*, 2014, pp. 388–396.

[42] S. Jayasumana, R. Hartley, M. Salzmann, H. Li, and M. T. Harandi, "Kernel methods on Riemannian manifolds with Gaussian RBF kernels," *IEEE Trans. Pattern Anal. Mach. Intell.*, vol. 37, no. 12, pp. 2464–2477, Dec. 2015.

[43] V. Arsigny, P. Fillard, X. Pennec, and N. Ayache, "Geometric means in a novel vector space structure on symmetric positive-definite matrices," *SIAM J. Matrix Anal. Appl.*, vol. 29, no. 1, pp. 328–347, 2007.

[44] S. Jung, I. Dryden, and J. Marron, "Analysis of principal nested spheres," *Biometrika*, vol. 99, pp. 551–568, 2012.

[45] Z. Huang, R. Wang, S. Shan, X. Li, and X. Chen, "Log-Euclidean metric learning on symmetric positive definite manifold with application to image set classification," in *Proc. Int. Conf. Mach. Learn.*, 2015, pp. 720–729.

[46] X. Pennec, P. Fillard, and N. Ayache, "A Riemannian framework for tensor computing," *Int. J. Comput. Vis.*, vol. 66, pp. 41–66, 2006.

[47] S. Sra, "A new metric on the manifold of kernel matrices with application to matrix geometric means," in *Proc. Int. Conf. Neural Inf. Process. Syst.*, 2012, pp. 144–152.

[48] S. Jayasumana, R. Hartley, M. Salzmann, H. Li, and M. T. Harandi, "Combining multiple manifold-valued descriptors for improved object recognition," in *Proc. Int. Conf. Digit. Image Comput. Tech. Appl.*, 2013, pp. 1–6.

[49] Y. Hu, A. S. Mian, and R. Owens, "Sparse approximated nearest points for image set classification," in *Proc. IEEE Int. Conf. Comput. Vis.*, 2011, pp. 121–128.

[50] A. Edelman, T. A. Arias, and S. T. Smith, "The geometry of algorithms with orthogonality constraints," *SIAM J. Matrix Anal. Appl.*, vol. 20, pp. 303–353, 1998.

[51] R. A. Fisher, "The use of multiple measurements in taxonomic problems," *Ann. Eugenics*, vol. 7, pp. 179–188, 1936.

[52] M. Kim, S. Kumar, V. Pavlovic, and H. Rowley, "Face tracking and recognition with visual constraints in real-world videos," in *Proc. IEEE Conf. Comput. Vis. Pattern Recognit.*, 2008, pp. 1–8.

[53] L. Wolf, T. Hassner, and I. Maoz, "Face recognition in unconstrained videos with matched background similarity," in *Proc. IEEE Conf. Comput. Vis. Pattern Recognit.*, 2011, pp. 529–534.

[54] J. R. Beveridge, et al., "The challenge of face recognition from digital point-and-shoot cameras," in *Proc. Int. Conf. Biometrics: Theory Appl. Syst.*, 2013, pp. 1–8.

[55] Z. Huang, et al., "A benchmark and comparative study of video-based face recognition on COX face database," *IEEE Trans. Image Process.*, vol. 24, no. 12, pp. 5967–5981, Dec. 2015.

[56] J. Beveridge, et al., "Report on the FG 2015 video person recognition evaluation," in *Proc. Int. Conf. Autom. Face Gesture Recognit. Workshop*, 2015, pp. 1–8.

[57] R. Wang and X. Chen, "Manifold discriminant analysis," in *Proc. IEEE Conf. Comput. Vis. Pattern Recognit.*, 2009, pp. 429–436.

[58] M. Hayat, M. Bennamoun, and S. An, "Deep reconstruction models for image set classification," *IEEE Trans. Pattern Anal. Mach. Intell.*, vol. 37, no. 4, pp. 713–727, Apr. 2015.

[59] T. Kim, J. Kittler, and R. Cipolla, "Discriminative learning and recognition of image set classes using canonical correlations," *IEEE Trans. Pattern Anal. Mach. Intell.*, vol. 29, no. 6, pp. 1005–1018, Jun. 2007.

[60] H. Cevikalp and B. Triggs, "Face recognition based on image sets," in *Proc. IEEE Comput. Soc. Conf. Comput. Vis. Pattern Recognit.*, 2010, pp. 2567–2573.
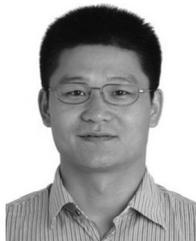
Zhiwu Huang received the BS degree in computer science and technology from Huaqiao University, Quanzhou, Fujian, China, in 2007, and the MS degree in computer software and theory from Xiamen University, Xiamen, Fujian, China, in 2010, and the PhD degree in computer science and technology from the Institute of Computing Technology (ICT), Chinese Academy of Sciences (CAS), Beijing, China, in 2015. He is currently a postdoctoral researcher in the Computer Vision Laboratory, Swiss Federal Institute of Technology (ETH) in Zurich, Switzerland, since September 2015. His research interests include computer vision, Riemannian computing, metric learning, and deep learning. He is a member of the IEEE.
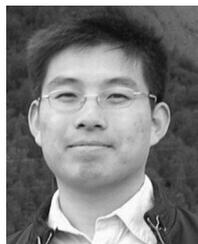
Ruiping Wang received the BS degree in applied mathematics from Beijing Jiaotong University, Beijing, China, in 2003 and the PhD degree in computer science from the Institute of Computing Technology (ICT), Chinese Academy of Sciences (CAS), Beijing, in 2010. He was a postdoctoral researcher in the Department of Automation, Tsinghua University, Beijing, from July 2010 to June 2012. He also spent one year working as a research associate in the Computer Vision Laboratory, Institute for Advanced Computer Studies, University of Maryland, College Park, from November 2010 to October 2011. He has been with the faculty of the Institute of Computing Technology, Chinese Academy of Sciences, since July 2012, where he is currently an associate professor. His interests include computer vision, pattern recognition, and machine learning. He is a member of the IEEE.

Shiguang Shan received the MS degree in computer science from Harbin Institute of Technology, Harbin, China, in 1999 and the PhD degree in computer science from the Institute of Computing Technology (ICT), Chinese Academy of Sciences (CAS), Beijing, China, in 2004. He joined ICT, CAS in 2002 and has been a professor since 2010. He is now the deputy director of the Key Lab of Intelligent Information Processing of CAS. His research interests cover computer vision, pattern recognition, and machine learning. He especially focuses on face recognition related research topics. He has published more than 200 papers in refereed journals and proceedings in the areas of Computer Vision and Pattern Recognition. He has served as area chair for many international conferences including ICCV'11, ICPR'12, ACCV'12, FG'13, ICPR'14, and ICASSP'14. He served as workshop co-chair of ACCV14, and website co-chair of ICCV'15. He is an associate editors of the *IEEE Transactions on Image Processing*, the *Neurocomputing*, the *Pattern Recognition Letters*, and the *Computer Vision and Image Understanding*. He received the China's Natural Science Awards in 2015 for his work on visual information processing and learning. He is a senior member of the IEEE.

Luc Van Gool received the degree in electro-mechanical engineering from Katholieke Universiteit Leuven, in 1981. Currently, he is a full professor for computer vision with the ETH in Zurich and the Katholieke Universiteit Leuven in Belgium. He leads research and teaches at both places. He has authored more than 300 papers in his field. He has been a program committee member of several, major computer vision conferences (e.g., program chair ICCV'05, Beijing, and general chair of ICCV'11, Barcelona, and of ECCV'14, Zurich). His main interests include 3D reconstruction and modeling, object recognition, and tracking and gesture analysis. He received several Best Paper awards (eg. David Marr Prize '98, Best Paper CVPR'07, Tsuji Outstanding Paper Award ACCV'09, Best Vision Paper ICRA'09). In 2015 he received the 5-yearly Excellence Prize for Applied Sciences from the Flemish Institute for Scientific Research (FWO). He is a co-founder of about 10 spin-off companies. He is a member of the IEEE.

Xilin Chen received the BS, MS, and PhD degrees in computer science from the Harbin Institute of Technology, Harbin, China, in 1988, 1991, and 1994, respectively. He was a professor with the Harbin Institute of Technology from 1999 to 2005. He was a visiting scholar with Carnegie Mellon University, Pittsburgh, Pennsylvania, from 2001 to 2004. He has been a professor with the Institute of Computing Technology, Chinese Academy of Sciences (CAS), since August 2004. He is the director of the Key Laboratory of Intelligent Information Processing, CAS. He has published one book and more than 200 papers in refereed journals and proceedings in the areas of computer vision, pattern recognition, image processing, and multimodal interfaces. He is a leading editor of the *Journal of Computer Science and Technology*, and an associate editor in chief of the *Chinese Journal of Computers*. He served as an Organizing Committee / Program Committee Member for more than 50 conferences. He is a recipient of several awards, including the China's State Scientific and Technological Progress Award in 2000, 2003, 2005, and 2012 for his research work. He is a fellow of the IEEE and the China Computer Federation (CCF).

▷ **For more information on this or any other computing topic, please visit our Digital Library at** www.computer.org/publications/dlib.